Nonlinear light-matter interaction with femtosecond high-angle Bessel beams

D. Faccio,[1,2,*] E. Rubino,[2] A. Lotti,[2,3] A. Couairon,[3] A. Dubietis,[4] G. Tamošauskas,[4] D. G. Papazoglou,[5,6] and S. Tzortzakis[5,6]

[1]*School of Engineering and Physical Sciences, SUPA, Heriot-Watt University, Edinburgh EH14 4AS, UK*

[2]*Dipartimento di Scienza e Alta Tecnologia, Università dell'Insubria, Via Valleggio 11, I-22100 Como, Italy*

[3]*Centre de Physique Theorique CNRS, Ecole Polytechnique, F-91128 Palaiseau, France*

[4]*Department of Quantum Electronics, Vilnius University, Sauletekio Avenue 9, Building 3, LT-10222 Vilnius, Lithuania*

[5]*Institute of Electronic Structures and Laser, Foundation for Research and Technology Hellas, P.O. Box 1527, 71110 Heraklion, Greece*

[6]*Materials Science and Technology Department, University of Crete, 71003 Heraklion, Greece*

(Received 22 December 2011; published 23 March 2012)

We show that high-angle Bessel beams may significantly reduce nonlinear pulse distortions due, for example, to nonlinear Kerr effects (self-phase-modulation and self-focusing) yet enhance ionization and plasma generation. Holographic reconstruction of Bessel beams in water show intensity clamping at increased intensities and evidence of nontrivial plasma dynamics as the input energy is increased. The solvated electron density increases significantly and the cavitation-induced bubbles are ejected from the focal region indicating a significant excess plasma heating in the Bessel-pulse wake.

DOI: 10.1103/PhysRevA.85.033829 PACS number(s): 42.65.Re, 42.65.Hw

Focused femtosecond pulsed laser beams with a Gaussian transverse spatial profile and high input powers propagating in a transparent isotropic medium undergo a series of nonlinear effects related to the third-order nonlinearity, to multiphoton absorption and ionization combined with dispersion and diffraction. The sum of these effects can lead to a dramatic reshaping of the laser beam itself that may either breakup under the effect of the modulational instability or form a filament [1]. In some circumstances this transformation may be beneficial (e.g., ultrashort laser pulse filaments and the laser pulse supercontinuum have found a wide range of applications [1–3]), but in others these may lead to a severe degradation of the expected laser pulse features at the focus in terms of maximum intensity or beam localization.

Nonlinear Kerr-induced phase distortions lead to frequency broadening and self-focusing. These are "cumulative" effects in the sense that they require propagation (i.e., dispersion and diffraction) in order for the Kerr-induced phase-distortions to accumulate and thus dramatically modify the pulse and/or beam profile [4–6]. Alongside nonlinear propagation effects on the pulse, important modifications occur also within the medium itself, namely plasma generation via multiphoton ionization. Laser-induced plasma strings are important for a variety of applications (e.g., for fundamental light-matter interaction studies, spectroscopy, controlled electric discharge, and temporary and permanent modification of transparent solids [2,7–10]). Finally, a rather general result of the interplay of all these effects, independently of the medium chosen (e.g., gas, liquid, or solid) is a clamping of the maximum intensity reached by the laser pulse during propagation [11,12]. With loose focusing conditions, typical clamped intensity values are of the order of 100 TW/cm^2 in air and 1 TW/cm^2 in water. Any attempt to increase the focus intensity beyond the clamped value by simply increasing the input energy will result in either a longer filamentation region with multiple temporal pulse splitting events or spatial breakup into multiple filaments [1].

Alternatively a tighter focusing geometry may be employed: increasing the focusing numerical aperture (NA) will eventually lead to a situation in which intensity clamping is overridden leading to an optical damage of the medium [13] although high intensities (and plasma densities) are reached only in very small, sub-μm^3 volumes [14–16].

In this work we investigate the interaction of high-intensity femtosecond laser pulses focused into a sample of water with a high-angle conical lens or axicon so as to form a Bessel beam. We study the impact of using relatively large Bessel angles in condensed media and show that alongside a strong reduction in Kerr-induced temporal and spectral pulse distortions, the maximum clamping intensity may be effectively increased beyond the value expected for a Gaussian pulse focused with the same NA. The effects of the higher intensities reached by the high-angle Bessel beam are directly monitored by measuring the plasma density and nonlinearly induced refractive-index profile by the femtosecond Bessel pulse using a holographic reconstruction technique. The measurements show a strong revival of the refractive-index changes induced by the plasma after an initial recombination process with a delay that is reduced with increasing input pulse energy. We ascribe this to excess heating of the plasma electrons, evidence of which is found also in the high transverse velocity of cavitation bubbles that appear to be ejected away from the plasma region.

We first consider the effect of a conical focusing geometry on Kerr-induced pulse-reshaping effects. A schematic representation of the Bessel-beam interaction geometry is shown in Fig. 1(a): nonlinear effects occur only within the hot, intense core [17,18] with diameter D given by the diameter of the central Bessel peak (e.g., measured between the first two zeros). Therefore an external annular region will propagate linearly toward the axis and will suffer nonlinear effects only when it traverses the central core region (i.e., over a distance given by $L = D/\sin\theta$ and θ is the Bessel angle). For example, for a $\theta = 7^\circ$ Bessel beam at 800-nm wavelength, we have $L \sim 16$ μm, which is much smaller than the nonlinear Kerr length over which distortions of the pulse due to Kerr effects will occur, $L_{\rm nl} = 1/(k_0 n_2 I_p) \sim 50$–$100$ μm, where k_0 is the

*d.faccio@hw.ac.uk

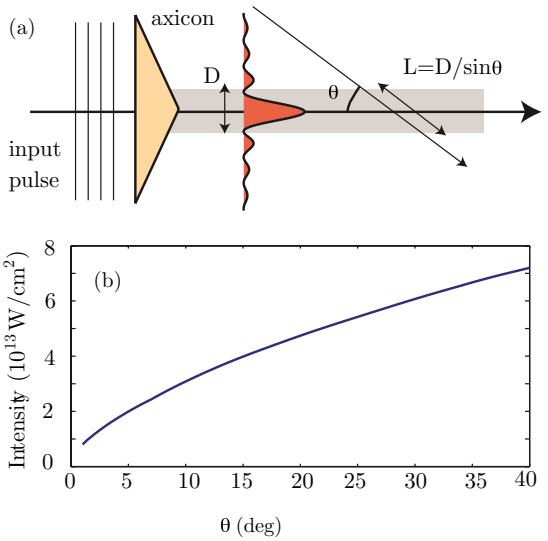

FIG. 1. (Color online) (a) Scheme of axicon focusing layout. (b) Maximum intensity with input energy 400 μJ and for increasing Bessel angle predicted by the model described in the text.

input beam wave vector, $n_2 = 2.7 \times 10^{-16}$ cm^2/W [19,20] is the nonlinear Kerr index of water, and $I_p \sim (0.5\text{–}1) \times 10^{13}$ W/cm^2 is the pulse peak intensity. In other words, we expect high focusing angles to suppress pulse distortions due to nonlinear propagation, yet this will be truly effective only if we remove the on-axis components of the beam, as proposed here using a high-angle conical focusing element. We note that this a very different situation with respect to the low-angle and highly nonlinear Bessel beams investigated, for example, in Refs. [21–24].

We now note that ionization and plasma generation only depend on the local pulse intensity I_p and will not be affected by axicon focusing [25,26]. Indeed, we show with a simple model that I_p is actually expected to increase with θ in the axicon focusing configuration.

As argued above, the Kerr effects are all the more negligible as the Bessel angle is increasing and plasma defocusing is not efficient for a Bessel beam. Intensity clamping is therefore determined by the balance between the absorption rate within the Bessel hot core (due to multiphoton ionization) and the inward energy flux from the surrounding reservoir toward the hot core. We note that additional pulse-reshaping effects related to propagation [27] are negligible here. Indeed, the central peak of the Bessel beam does not suffer diffraction or the same phase evolution of a Gaussian beam as it is the result of a continuously reconstructed interference pattern. In the nonlinear regime, the Bessel beam may propagate stationarily because there is a flux of energy from the tail toward the main lobe where intensity is high and multiphoton absorption acts as a sink for energy [28,29]. We consider an input Gaussian beam with peak intensity I_0, width w_0 ($1/e^2$), pulse duration at full-width-half-maximum T. If we focus this beam with an axicon with base angle γ, which corresponds to a Bessel cone angle θ, we obtain a beam with a Bessel profile $J_0(k_0 \sin\theta\, r)$ over the Bessel zone of length $L_{\rm BB} = w_0/\tan\theta$. For simplicity, we assume that the peak intensity I_p of the Bessel beam is constant over the Bessel zone. We assume that the Bessel beam dissipates a certain fraction x of the energy flux (this corresponds to the unbalance between the inward and outward components of the nonlinear Bessel beam) and the dissipated energy per unit length (i.e., energy flux) is $x E_{\rm in}/L_{\rm BB}$.

Now we compute the energy dissipated in the core of the Bessel beam. From the standard nonlinear Schrödinger propagation equation [1], we calculate the evolution of the intensity ($\partial I/\partial z$) and integrate in space and time to obtain the energy flux

$$\frac{\partial \iint I dt 2\pi r dr}{\partial z} = -\beta_K \iint I^K dt 2\pi r dr, \qquad (1)$$

where K is the order (number of involved photons) and β_K is the coefficient of the multiphoton absorption. The energy lost per unit length in the core of the Bessel beam is

$$\frac{E_{\rm lost}}{L_{\rm BB}} = \beta_K I_p^K \frac{T}{\sqrt{2\ln 2}} \frac{\sqrt{\pi}}{\sqrt{2K}} \frac{2\pi}{k_0^2 \sin^2\theta} \int_0^{u_0} J_0^{2K}(u) u du, \qquad (2)$$

where u_0 denotes the first zero of the Bessel function (nonlinear losses are assumed to occur only in the main lobe [17]). If we want to reach a given intensity I_p, we must use an axicon that has a cone angle larger than a certain threshold given by $x E_{\rm in}/L_{\rm BB} = E_{\rm lost}/L_{\rm BB}$ [i.e., the inward energy flux must be equal to (or higher than) that lost in the central core region]. This condition gives

$$\tan\theta \sin^2\theta = \frac{\beta_K g(K)}{n_0^2} \frac{T w_0 \lambda_0^2 I_p^K}{x E_{\rm in}}, \qquad (3)$$

where the pulsed-Bessel shape factor is defined as $g(K) = \int_0^{u_0} J_0^{2K}(u) u du/(4\sqrt{\pi K \ln 2})$. In Fig. 1(b) we show the result of this last relation expressed in terms of the highest achievable intensity as a function of the Bessel angle θ. This curve was calculated for an input Gaussian pulse with 800 nm, $T = 40$ fs, $w_0 = 4$ mm, $E_{\rm in} = 400$ μJ, and water medium with $K = 5$, $\beta_5 = 8.3 \times 10^{-50}$ cm^7/W^4. We also take $x = 1$ (i.e., we assume the limiting case in which all of the incoming energy is absorbed in the highly nonlinear region close to the central Bessel peak). This condition consequently determines the highest possible peak intensity that can be reached for a given input angle. We note that the model therefore predicts that by increasing the angle of the Bessel the maximum clamping intensity may be shifted to significantly higher values with respect to a Gaussian pulse ($\sim 1 \times 10^{13}$ TW/cm^2) and in any case, well within the tunneling ionization regime $I \gtrsim 2 \times 10^{13}$ TW/cm^2.

We performed measurements using a $\gamma = 20^\circ$ base angle, fused silica axicon ($\theta = 7^\circ$ Bessel angle in water) to focus a Gaussian pulse with 40-fs duration, 800-nm wavelength, 4-mm input waist radius into a 3-cm long water sample. The input energy was varied up to 1.85 mJ. We observed that a Gaussian pulse (focused using a standard microscope objective with NA = 0.11, close to that of the axicon) generated very intense white light, even at the lowest energies, while the axicon focusing generated no observable spectral broadening even at the high $\sim$1 mJ energies, indicating a suppression of the Kerr-induced temporal and spectral dynamics.

Plasma generation was characterized by a holographic microscopy technique that allows to reconstruct the full spatial profile of both the real δn and imaginary $\delta\kappa$ components of the

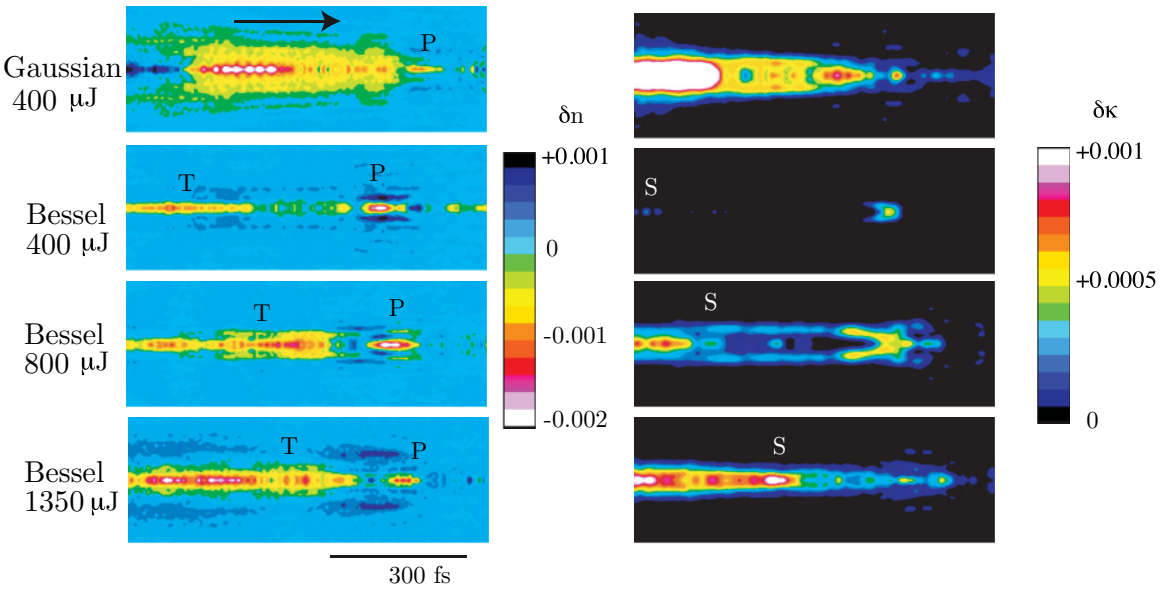

FIG. 2. (Color online) Measured refractive-index variations (real part δn in the left hand panel, imaginary part $\delta\kappa$ in the right hand panel) induced by the laser pulse under the input conditions (beam profile and energy) as indicated in the figure. P indicates the pulse position, T the solvated electron tail and S the position of the onset of thermalized solvated electron-induced absorption.

total refractive-index variation. The diffraction pattern induced on a normal-incidence probe pulse is recorded at six different distances from the water cell and these are then used to numerically retrieve δn and $\delta\kappa$. The spatial and temporal resolutions are limited by the wavelength and duration of the probe pulse to 1 μm and 40 fs, respectively. A detailed description of this method is given by the authors of Refs. [30,31]. Figure 2 shows the plasma (negative) $|\delta n|$ (left-hand panel) and $\delta\kappa$ (right-hand panel) for 0.4, 0.8, and 1.35 mJ input energies and also for an equivalent-NA Gaussian beam at 400 μJ. The actual laser peak position is indicated with P. The peak δn and plasma density ρ values measured in correspondence to the laser pulse are shown in Fig. 3. The plasma density was calculated from the measured refractive-index values using a simple Drude model (a detailed description of the approach we use to isolate the refractive-index changes induced by plasma is provided in Ref. [32]). These plasma densities can be used to estimate the pulse peak intensity (assuming a 40-fs Gaussian temporal profile and integrating over the pulse with ionization included through the Keldysh multiphoton ionization rates). An agreement within a factor two is found with the intensities predicted by our simple model.

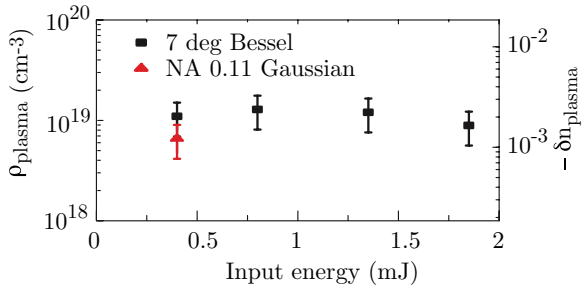

FIG. 3. (Color online) Plasma density and relative refractive-index variation retrieved from the holographic measurements for four different input energies (corresponding to position P in Fig. 2).

The Bessel beam induces a δn that is roughly two time larger than that of the Gaussian beam. Most interestingly, as we increase the Bessel intensity the trailing refractive-index variation, indicated with T in Fig. 2, shows a marked increase. This tail is due to solvated electrons [i.e., plasma electrons captured by the water polar molecules with long life-times (>100 ps)] [33–35]. At low input energies, the measured delay ~300 fs between the main pulse and the creation of the solvated electron population agrees well with the same time measured by other methods [33]. We note that it is possible to isolate plasma generation from electron solvation due to the very different temporal dynamics involved. The electrons forming the plasma have an average recombination time of roughly 100 fs after which we expect the laser-pulse-induced plasma to disappear. On the other hand, electron solvation requires at least 300 fs to occur. So this effect will switch on well after the plasma has switched off. Indeed, in our measurements we clearly see a "dead-time" between 100 and 300 fs in which no refractive-index modification is visible. Furthermore, in the imaginary part of the refractive-index change $\delta\kappa$ (Fig. 2) we observe a clear signature of the electron thermalization correlated to the characteristic absorption [36] that occurs about 300 fs later (i.e., at a delay of ~600 fs). However, we also note that this time decreases with increasing energy: the position of S in Fig. 2 indicates the onset of solvated electron absorption, which is seen to shift by ~400 fs when increasing the input energy from 400 to 1350 μJ. While the actual pulse δn does not increase with input energy (indicating intensity clamping, albeit at a higher intensity with respect to the Gaussian beam), the onset of solvated electron absorption decreases significantly. Previous studies have shown how an increase in temperature will lead to a decrease in the electron thermalization times [37], and hence also in the onset of absorption. We thus interpret the observed change in the temporal dynamics of the absorption properties as an indication that the larger input energies are leading to a

plasma with similar densities (due to intensity clamping), but characterized by increased electron temperatures.

We also note that, when compared to the Bessel plasma distribution, the Gaussian pulse is clearly losing energy through multiphoton ionization over a much larger volume that extends well beyond the axial region. This observation indeed represents one of the main differences between the behavior of the Bessel and Gaussian beams. Gaussian pulses have a large part of the energy at low angles with respect to the propagation axis and suffer nonlinear effects over significantly larger distances and areas: increasing the input energy above a certain clamping threshold does not lead to an increase of the peak intensity, but rather to an increase of the overall volume within which nonlinear effects, in particular nonlinear losses and ionization, occur and energy is deposited prior to the focus [38]. Conversely, in Bessel beams the energy is directed at large angles toward the axis and propagates linearly until the central core region is reached. It is only here that significant nonlinear effects occur (i.e., within a volume that remains approximately constant with increasing energy). Bessel beams therefore allow for a higher clamping intensity compared to Gaussian beams of similar NA because plasma defocusing is inefficient on the conical components.

We also note that complicated multifilament structures associated to the Gaussian pulse introduce inaccuracies when applying the cylindrically symmetric Abel transform, as used here to estimate the spatial distribution of the refractive index from the holographic images. Thus, useful quantitative information can be obtained only for low Gaussian pulse energies (as shown here and in Refs. [34,35]).

In Fig. 4(a) we show transmission measurements for the 7° Bessel beam (solid line) and equivalent-NA Gaussian beam (dashed line) with increasing input energy. The Gaussian beam shows a continuous increase in the nonlinear absorption that saturates around 50–500 μJ, due to clamping of the maximum intensity and hence also of the nonlinear losses.

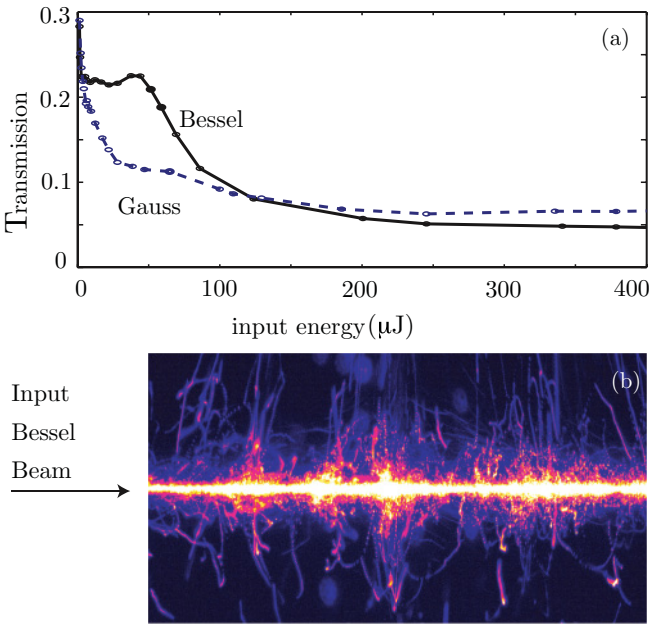

FIG. 4. (Color online) (a) Transmission measurements. (b) A side view of the Bessel filament and transversally ejected bubbles.

The Bessel beam shows a significantly different behavior: at input energies around 60 μJ, which according to Eq. (3) also correspond to the predicted saturation intensity $\sim$20 TW/cm^2, the transmission curve shows a sudden increase, followed by a further decrease. We attribute this nonmonotonic behavior of the transmission to a spurious effect that, however, is still related to the dynamics considered here: cavitation and subsequent bubble ejection from the focal region. Indeed, as a first test we verified that the transmission peak disappeared when lowering the laser repetition rate from 1 kHz down to 2–50 Hz. However, in all cases bubbles are formed, down to energies of a few μJ, indicating that these are generated as a result of laser-pulse-induced cavitation (and not to heating of the medium). Moreover, the bubbles could be clearly seen to be ejected transversally at energies $>$60 μJ: a side view of the Bessel zone, taken with a CCD camera and 50-ms exposure (corresponding to 50 laser pulses at 1 kHz repetition rate, each with 200 μJ energy) is shown in Fig. 4(b): the horizontal bright stripe is due to scattering from the nonlinear extended focal region of the Bessel beam [17], propagating here from left to right. The traces directed along the vertical directions are left by the ejected bubbles. We tentatively attribute these traces as due to an increase in the plasma temperature at higher input energies that in turn leads to enhanced expansion forces within the medium and thus to bubble ejection. These bubbles are illuminated by successive laser pulses at a 1-kHz repetition rate (i.e., the laser pulses act as a kHz stroboscopic illumination source). Therefore, by measuring the distance between successive bubble positions, each separated by a known time, 1 ms, the average bubble speed is estimated to be 1–10 cm/s.

For energies $\sim$60 μJ the bubbles are therefore ejected away by a distance 10–100 μm in 1 ms (i.e., they are ejected away from the main laser focal spot region well before the next laser pulse enters the medium). This provides an explanation for the apparent increase in transmission around 60 μJ. At lower input energies cavitation (without bubble ejection) leads to the formation on-axis of very slowly moving bubbles (i.e., that move only under buoyancy effects). These practically static bubbles scatter light from successive laser pulses and therefore lead to a decrease in the transmission when this is measured as an average over many laser shots. At higher input energies, the bubbles are ejected away from the on-axis region [see Fig. 4(b)] as a result of the higher temperature plasma and therefore do not affect successive laser pulses in the same way: the transmission tends to return to the values it would have in a hypothetical situation in which no bubbles are generated. This gives the impression of a net increase in the transmission. We note that the ejected bubbles still remain within the overall Bessel diameter for the successive four to five laser shots. The bubble spatial distribution is now significantly altered with respect to low input energies. We pass from a situation (at low energies) with a long, nearly continuous distribution of on-axis bubbles that lead to very strong scattering, to a situation in which the bubbles are dispersed to different radial positions (i.e., similar to a distribution of very small, random scatterers). This represents a major difference for Bessel beams as these are known to have remarkable reconstruction properties that allow them to reform nearly immediately after a scatterer and ultimately to propagate through a random scattering medium. However, the condition for this is that indeed we have a random

or sparse scatterer distribution: a single, nearly continuous and extended scattering object such as that generated at low input energies will not allow the Bessel beam to reform and will thus give rise to enhanced scattering losses.

We also noted that the bubble ejection was nearly absent or extremely weak with Gaussian pulses at all energies up to 1.8 mJ. We therefore conclude that a clearly different process is occurring when pumping with a Bessel beam. We ascribe this difference to the aforementioned excess plasma heating obtained with the Bessel beam. Indeed, a higher electron temperature that would explain the higher solvated electron density in Fig. 2 would also imply a stronger shock wave induced by plasma heating that could lead to bubble ejection out of the focal zone.

In conclusion, high-angle ultrashort pulsed Bessel beams on the one hand enable a strong reduction of Kerr-like effects (e.g., self-phase-modulation and self-focusing) and on the other enhance ionization and laser-induced plasma effects. These findings are supported by simple models and by experimental results that show clear differences with respect to Gaussian beams focused with the same NA. In particular, axicon focusing leads to strong or nearly complete suppression of Kerr-induced white-light generation, a higher peak intensity limit and significantly different plasma dynamics. Above the intensity clamping limit, the solvated electron density starts to increase indicating a possibly higher electron temperature within the laser-induced plasma. This increase in temperature would also explain the rather remarkable bubble ejection we have reported. Further studies at higher Bessel angles and/or energies are expected to shed more light on the physics at play and on the electron heating mechanism, which are also expected to play an important role for example in micromachining or biomedical applications [39–42].

This work was supported by the EU MC Excellence Grant "MULTIRAD," Grant No. MEXTCT-2006-042683.

[1] A. Couairon and A. Mysyrowicz, Phys. Rep. **441**, 47 (2007).
[2] S. L. Chin, *Femtosecond Laser Filamentation* (Springer, New York, 2010).
[3] *The Supercontinuum Laser Source*, 2nd ed. edited by R. R. Alfano (Springer, New York, 2006).
[4] J. K. Ranka, R. W. Schirmer, and A. L. Gaeta, Phys. Rev. Lett. **77**, 3783 (1996).
[5] A. Dubietis, E. Gaižauskas, G. Tamošauskas, and P. Di Trapani, Phys. Rev. Lett. **92**, 253903 (2004).
[6] A. Matijošius, J. Trull, P. Di Trapani, A. Dubietis, R. Piskarskas, A. Varanavičius, and A. Piskarskas, Opt. Lett. **29**, 1123 (2004).
[7] A. L. Gaeta, Science **301**, 54 (2003).
[8] J. Kasparian, M. Rodriguez, G. Méjean, J. Yu, E. Salmon, H. Wille, R. Bourayou, S. Frey, Y.-B. André, A. Mysyrowicz, R. Sauerbrey, J.-P. Wolf, and L. Wöste, Science **301**, 61 (2003).
[9] S. Tzortzakis, D. G. Papazoglou, and I. Zergioti, Opt. Lett. **31**, 796 (2006).
[10] D. G. Papazoglou, I. Zergioti, and S. Tzortzakis, Opt. Lett. **32**, 2055 (2007).
[11] J. Kasparian, R. Sauerbrey, and S. L. Chin, Appl. Phys. B **71**, 877 (2000).
[12] W. Liu, S. Petit, A. Becker, N. Aközbek, C. M. Bowden, and S. L. Chin, Opt. Commun. **202**, 189 (2002).
[13] S. Juodkazis, K. Nishimura, S. Tanaka, H. Misawa, E. G. Gamaly, B. Luther-Davies, L. Hallo, P. Nicolai, and V. T. Tikhonchuk, Phys. Rev. Lett. **96**, 166101 (2006).
[14] P. P. Kiran, S. Bagchi, S. R. Krishnan, C. L. Arnold, G. R. Kumar, and A. Couairon, Phys. Rev. A **82**, 013805 (2010).
[15] E. G. Gamaly, Phys. Rep. **508**, 91 (2011).
[16] F. Théberge, W. Liu, P. T. Simard, A. Becker, and S. L. Chin, Phys. Rev. E **74**, 036406 (2006).
[17] P. Polesana, D. Faccio, P. Di Trapani, A. Dubietis, A. Piskarskas, A. Couairon, and M. A. Porras, Opt. Express **13**, 6160 (2005).
[18] Z. Song and T. Nakajima, Opt. Express **18**, 12923 (2010).
[19] A. Couairon, E. Gaižauskas, D. Faccio, A. Dubietis, and P. Di Trapani, Phys. Rev. E **73**, 016608 (2006).
[20] A. Dubietis, A. Couairon, E. Kučinskas, G. Tamošauskas, E. Gaižauskas, D. Faccio, and P. Di Trapani, Appl. Phys. B **84**, 439 (2006).
[21] D. E. Roskey, M. Kolesik, J. V. Moloney, and E. M. Wright, Opt. Express **15**, 9893 (2007).
[22] P. Polynkin, M. Kolesik, A. Roberts, D. Faccio, P. Di Trapani, and J. Moloney, Opt. Express **16**, 15733 (2008).
[23] A. Dubietis, P. Polesana, G. Valiulis, A. Stabinis, P. Di Trapani, and A. Piskarskas, Opt. Express **15**, 4168 (2007).
[24] P. Polesana, M. Franco, A. Couairon, D. Faccio, and P. Di Trapani, Phys. Rev. A **77**, 043814 (2008).
[25] D. Abdollahpour, P. Panagiotopoulos, M. Turconi, O. Jedrkiewicz, D. Faccio, P. Di Trapani, A. Couairon, D. G. Papazoglou, and S. Tzortzakis, Opt. Express **17**, 5052 (2009).
[26] S. Akturk, B. Zhou, M. Franco, A. Couairon, and A. Mysyrowicz, Opt. Commun. **282**, 129 (2009).
[27] S. Polyakov, F. Yoshino, and G. Stegeman, J. Opt. Soc. Am. B **18**, 1891 (2001).
[28] P. Polesana, A. Dubietis, M. A. Porras, E. Kučinskas, D. Faccio, A. Couairon, and P. Di Trapani, Phys. Rev. E **73**, 056612 (2006).
[29] P. Polesana, A. Couairon, D. Faccio, A. Parola, M. A. Porras, A. Dubietis, A. Piskarskas, and P. Di Trapani, Phys. Rev. Lett. **99**, 223902 (2007).
[30] D. Abdollahpour, D. G. Papazoglou, and S. Tzortzakis, Phys. Rev. A **84**, 053809 (2011).
[31] D. G. Papazoglou and S. Tzortzakis, Appl. Phys. Lett. **93**, 041120 (2008).
[32] D. G. Papazoglou and S. Tzortzakis, Opt. Mater. Express **1**, 625 (2011).
[33] A. Migus, Y. Gauduel, J. L. Martin, and A. Antonetti, Phys. Rev. Lett. **58**, 1559 (1987).
[34] S. Minardi, A. Gopal, M. Tatarakis, A. Couairon, G. Tamošauskas, R. Piskarskas, A. Dubietis, and P. Di Trapani, Opt. Lett. **33**, 86 (2008).
[35] S. Minardi, A. Gopal, A. Couairon, G. Tamošauskas, R. Piskarskas, A. Dubietis, and P. Di Trapani, Opt. Lett. **34**, 3020 (2009).

[36] C. L. Thomsen, D. Madsen, S. R. Keiding, J. Thogersen, and O. Christiansen, J. Chem. Phys. **110**, 3453 (1999).
[37] D. Madsen, C. L. Thomsen, J. Thorgersen, and S. R. Keiding, J. Chem. Phys. **113**, 1126 (2000).
[38] D. M. Rayner, A. Naumov, and P. B. Corkum, Opt. Express **13**, 3208 (2005).
[39] Y. Matsuoka, Y. Kizuka, and T. Inoue, Appl. Phys. A **84**, 423 (2006).
[40] M. K. Bhuyan, F. Courvoisier, P. A. Lacourt, M. Jacquot, R. Salut, L. Furfaro, and J. M. Dudley, Appl. Phys. Lett. **97**, 081102 (2010).
[41] M. K. Bhuyan, F. Courvoisier, P. A. Lacourt, M. Jacquot, L. Furfaro, M. J. Withford, and J. M. Dudley, Opt. Express **18**, 566 (2010).
[42] E. Gaižauskas, E. Vanagas, V. Jarutis, S. Juodkazis, V. Mizeikis, and H. Misawa, Opt. Lett. **31**, 80 (2006).